Materials and Structures (2012) 45:1829–1847
DOI 10.1617/s11527-012-9873-7

ORIGINAL ARTICLE

Stress distribution and crack formation in full-scaled ultra-high strength concrete columns

Ippei Maruyama · Masahiro Suzuki · Ryoichi Sato

Received: 23 October 2011 / Accepted: 19 May 2012 / Published online: 19 June 2012
© RILEM 2012

Abstract Full-scaled model columns were placed both in summer and winter with an ultra-high strength concrete with a compressive strength more than 150 MPa, and stress distribution and cracking were experimentally evaluated. Specimens placed in summer exhibited cracks around the steel reinforcements which sometimes joined together. Specimens placed in winter showed, in addition to the cracks around the reinforcement, an internal crack perpendicular to the column axis as well as at the specimen surface. These cracks were found to be dependent on the temperature history due to hydration heat liberation and associated autogenous shrinkage strains. It was shown that the autogenous shrinkage of concrete increased when temperature after mixing was low and the maximum temperature during temperature history was high. This accounts for the numerous cracks found in the specimen placed in winter. Strain perpendicular to the axial direction was smaller than that of the axial direction implying the tensile stress due to autogenous shrinkage acting perpendicular to the axial direction as far as the autogenous shrinkage is isotropic. Finite element analysis confirmed the lateral stress due to autogenous shrinkage. Possible influences of autogenous shrinkage of ultra-high strength concrete on the structural performance include (1) early spalling of cover concrete and degradation of flexural strength, (2) degradation of bond and shear strength, and (3) prospect of longitudinal crack in center of the column and degradation of flexural strength.

Keywords Autogenous shrinkage · Ultra high-strength concrete · Cracking

I. Maruyama (✉)
Faculty of Engineering, Graduate School of Environmental Studies, Nagoya University, Building 3, No. 580, Furo-cho, Chikusa-ku, Nagoya 464-8603, Japan
e-mail: ippei@dali.nuac.nagoya-u.ac.jp

M. Suzuki
Technical Research Laboratory, P.S. Mitsubishi Co., 2-1-67, Kamomiya, Odawara 250-0875, Japan
e-mail: msuzuki@psmic.co.jp

R. Sato
Hiroshima University, 1-4-1, Kagamiyama, Higashi-Hiroshima 739-8527, Japan
e-mail: sator@hiroshima-u.ac.jp

1 Introduction

High-strength concrete shows a remarkable progress in the practical applications because it enables high-rise concrete structure, smaller cross-section for the load baring members and a highly durable structure as a result of its dense material structure. The design strength as high as 200 MPa was adopted in recent years and a continued development in its applicability is expected.

On the other hand, the high-strength concrete exhibits large autogenous shrinkage and brittle fractures. Hence the properties of the high-strength concrete have been studied mainly in terms of the

drawbacks. Control of cracking in high-strength concrete due to autogenous shrinkage is even more important than in the normal concrete because an excellent durability is expected owing to its dense material structure. In this background, a large number of studies have been devoted to the autogenous shrinkage of high-strength concrete with low water–cement ratios [10, 15, 17, 22–24] and its control [1, 7, 9, 16, 21].

However, the past studies generally dealt with the laboratory experiment and those dealt with problems with the full-scaled members, including temperature after mixing, temperature histories due to hydration heat liberation, its distribution in the member and its time-dependant behavior, were very few. Cracking problems have been so far discussed in terms of the possibility to occur around aggregates [11] and steel bars [8, 12, 13].

This study evaluates the stress and cracking of reinforced high-strength concrete full-size columns exposed to realistic conditions, and discusses their effects on the structural performance of the members.

2 Experiment

2.1 Materials

Materials used in the experiments are shown in Table 1. Cements were two types of the commercial silica fume cements, SFC1 and SFC2, comprising low-heat Portland cements of LC1 and LC2 and 10 % of inclusively-premixed silica fumes of SF1 and SF2. The mineral compositions of the low-heat Portland cements according to the Bogue calculation show no significant difference. Because the replacement ratio of SF1 and SF2 are the same, the variation of SFC1 and SFC2 is supposed to be within the same range as that of the commercial product. The fine aggregate S was a crushed sand from Ohtsuki, Yamanashi prefecture, Japan and the coarse aggregate G was a crushed stone from Morioka, Iwate prefecture, Japan.

2.2 Mix proportions

Four batches of concrete, B1 to B4, were mixed in total and the mix proportions are shown in Table 2. The B1 and B2 were mixed in summer while B3 and B4 were mixed in winter.

Table 1 Materials used in experiments

Material	Type/physical properties/ characteristic	Notation
Low heat Portland cement 1	Blaine value: 3600 cm^2/g, density: 3.22 g/cm^3 Mineral composition: C_3S: 29.1 %, C_2S: 50.1 %, C_3A: 4.3 %, C_4AF: 9.6 %	L1
Low heat Portland cement 2	Blaine value: 3600 cm^2/g, density: 3.22 g/cm^3 Mineral composition: C_3S: 28.4. %, C_2S: 50.7 %, C_3A: 4.8 %, C_4AF: 9.4 %	L2
Silica fume 1	Density: 2.24 g/cm^3, BET surface area: 17.1 m^2/g, SiO_2 content: 95 %	SF1
Silica fume 2	Density: 2.24 g/cm^3, BET surface area: 17.9 m^2/g, SiO_2 content: 95 %	SF2
Silica fume cement 1	90 % low heat cement 1 + 10 % silica fume 1	SFC 1
Silica fume cement 2	90 % low heat cement 2 + 10 % silica fume 2	SFC 2
Fine aggregate	Crushed sand, surface dry density: 2.63 g/cm^3, adsorption ratio: 2.5 %, F.M. 2.53, packing ratio: 54 %	S
Coarse aggregate	Crushed aggregate, surface dry density: 2.93 g/cm^3, adsorption ratio: 0.39 %, F.M. 6.66, packing ratio: 60.0 %, maximum size: 20 mm	G
Super plasticizer	Polycarboxylic acid type	SP
Anti-foaming agent	Polyalkylene glycol derivative type	D

The mix proportions are shown by the full-scaled column specimens and are equal such that the water to binder ratio of 0.15 and targeted slump flow of 650 ± 100 mm. Antifoaming agent was used to control air content within the targeted value of 2 ± 1 %. Consequently, both slump flow and air content were controlled within an acceptable range. Mixing was performed with a biaxial forced mixer.

2.3 Specimens

2.3.1 Model column specimen

Four types of model column specimens were prepared. Dimensions of a specimen with a deformed bar D41 are

Table 2 Mixture proportions

	Specimen	Notation	Base cement	Silica fume	W/B %	W kg/m^3	C	S	G	SF	SP $\%_{cmwt}$	D $\%_{cmwt}$	Air %	Slump flow mm	Temp. °C	Env. temp. °C
B1	C-D6S	SFLC1	LC1	SF1	15	155	930	451	932	103	2.6	0.6	1.4	715 × 715	29.0	29.0
B2	C-D41S	SFLC1	LC1	SF1	15	155	930	451	932	103	2.6	0.6	1.5	745 × 720	29.5	31.0
B3	C-D6W	SFLC2	LC2	SF2	15	155	930	451	932	103	2.6	0.6	2.4	730 × 710	14.5	8.0
B4	C-D41W	SFLC2	LC2	SF2	15	155	930	451	932	103	2.6	0.6	2.2	710 × 705	15.5	10.5

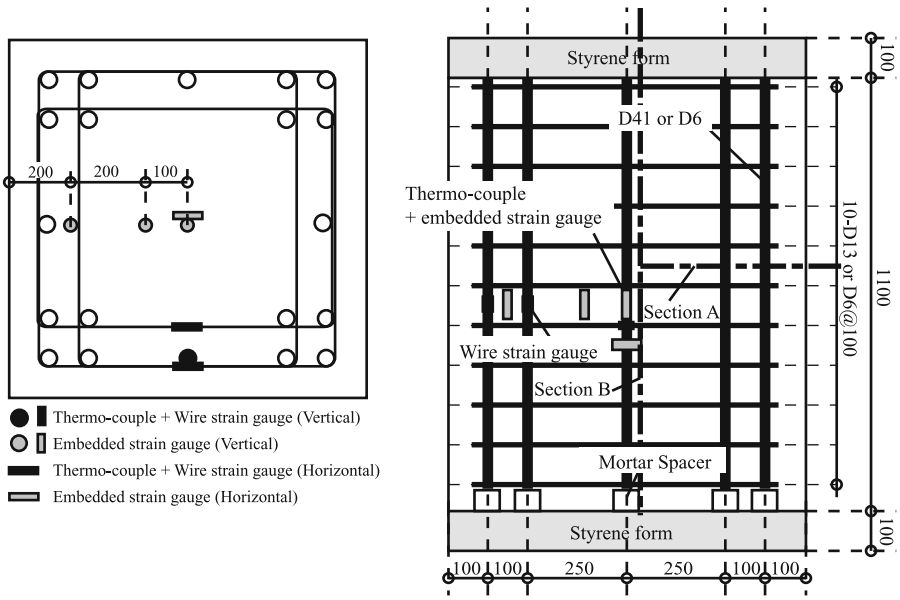

Fig. 1 Schematic of specimen

shown in Fig. 1. Among the model column specimens, temperature history and reinforcement ratio were varied. Temperature histories corresponding to summer and winter constructions were assumed and actual placement was executed in August and November. The dimensions of 900 × 900 × 1100 mm were common to all the specimen while arrangement of the main reinforcement was different: one used D41 for the main reinforcement and D13 for the shear reinforcement (denoted as C-D41, with a reinforcement ratio of 3.3 % and web reinforcement ratio of 0.14 %) and the other used D6 for the main and the shear reinforcement (denoted as C-D6, with a reinforcement ratio of 0.08 % and web reinforcement ratio of 0.14 %). The objective to introduce different reinforcement ratios for the main rebar is to discuss vertical strain history and distribution that must be altered by reinforcement in the columns. Mix proportions of concrete and their respective temperatures after mixing are shown in Table 2.

A foam polystyrene with a thickness of 100 mm was placed at the top and bottom of the column for thermal insulation. At the bottom of the column, mortar spacers were placed to avoid breakage of the foam. Metal form was used and, after placing, curing was performed with a sheet cover for 3 days. Then the specimen was demolded and placed in the experiment station. Temperatures were consecutively monitored at the surface of the mold, inside of the cover sheet and inside of the room. The experiments were carried out in the same room.

Strains and temperature history were measured with a mold type strain gauge (Ø20 × 104 mm with a rigidity of 40 N/mm^2) for concrete, a foil strain gauge for steel bars and a thermocouple at the same position. All the strain gauges were calibrated in advance for temperature compensation.

The mold type strain gauge was set vertically at the center while another one was additionally set horizontally 30 cm from the bottom for the summer specimen to study the strain of the horizontal direction and the difference in temperature as shown in Fig. 1.

The specimens were cut with a diamond cutter at the age of 28 days to observe the cross section of A and B as shown in Fig. 1. Internal cracks formed at early ages were visually observed during evaporation of applied water and acetone.

2.3.2 *Test of properties*

Specimens for testing the properties of concrete, such as compressive strength, elastic modulus, split tensile strength and autogenous shrinkage, were prepared under different temperature histories and humidity conditions. Specimens for compressive strength and elastic modulus measurement were identical and had a dimension of ∅100 × 200 mm. They were cured in different manners: a sealed curing in the same cover sheet as that of the column specimen, a quasi adiabatic sealed curing under expanded polystyrene box with sufficient heat insulation capability and the standard under water curing. In addition, cored specimens taken from the center of a column specimen were prepared at the age of 28-day. These four types of specimens were subjected to compressive strength and elastic modulus measurement.

Specimens for split tensile strength had a dimension of ∅150 × 200 mm and were cured in the same manner as that of the compressive strength and elastic modulus.

Specimens for autogenous shrinkage test had a dimension of 100 × 100 × 400 mm and were subjected to measurement immediately after mixing using a mold-type strain gauge embedded at the center section. A polyester film and a Teflon sheet were placed between specimen and the mold to reduce frictions. Unmolded 1 day after mixing, the specimen was sealed with aluminum foil for the subsequent measurement. Specimens were subjected to sealed curing in the same cover sheet as that of the column specimen at a room temperature. The thermal strain was calculated assuming a constant thermal expansion coefficient of 10×10^{-6}/°C for concrete specified as the design value for the normal concrete [5]. Autogenous shrinkage strains of concrete subjected to a high temperature history were determined for another batches of concretes, with the same mix proportions and a temperature after mixing of 10, 20 and 30 °C, that were cured under a quasi adiabatic condition in a box of expanded polystyrene [18].

In the present paper, "autogenous strain" is defined as the strain mainly caused by cement hydration reactions and resultant desiccation in the matrix and "thermal strain" is defined as the strain mainly caused by temperature change. In a precise sense, strain of cement paste or concrete is essentially a physical response of external and internal of finite element and it can not be separated, but in engineering manner for evaluating strain of concrete, apparent separation is useful in understanding the mechanism behind the phenomena and numerical calculations. Additionally, though it has been reported that thermal expansion coefficient in high strength concrete is increased due to self-desiccation, constant value is adopted for this study. In the present study, stress, strain and resultant cracks in full-size column are mainly focused, and for this purpose, the total strain of concrete is the matter of concern. For evaluating or predicting total strain of concrete, constant value of thermal expansion coefficient will not be problematic.

2.4 Results

2.4.1 *Compressive strength, elastic modulus and splitting tensile strength*

Development of compressive strength of the specimen as a function of effective material age based on CEB-FIP MC90 [2] is shown in Fig. 2. The temperature histories of the specimens with sealed and quasi-adiabatic curing as well as that of the cored specimen are shown in Fig. 3. Compressive strength of the specimens placed in summer can be arranged in a single curve as shown in Fig. 2 and can be treated as a single function of time regardless of the curing method. However, those placed in winter have to be compiled in two different functions, particularly for those subjected to the standard curing and to the other curing methods. Because the strain in reinforcing steel was first observed at the age of 0.4 days, as discussed later with Figs. 7 and 9, this effective age was assumed to be the point of origin and the following equation was adopted for compressive strength development.

$$f_c = a \exp\left(b\left(1 - (28/(t - 0.4))^{0.5}\right)\right) \quad (1)$$

where a is a coefficient regarding the final strength (MPa), b is a coefficient regarding strength

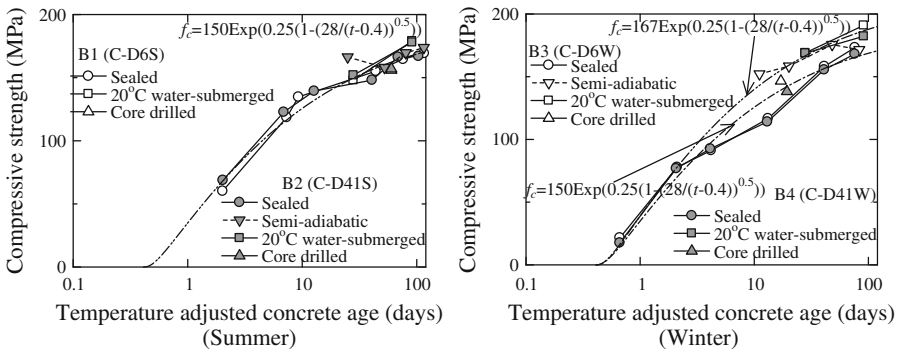

Fig. 2 Development of compressive strength of specimen placed in summer and winter. Relative standard deviation of compressive strength and Young's modulus is 2.66 and 2.88 % respectively

development, t is effective age (day) and f_c is compressive strength (MPa).

Specimens placed in summer attained the same strength level in any curing conditions of the standard curing or the sealed curing while those placed in winter showed a higher strength when subjected to the standard curing. The investigation of the reason remains as a task for the future.

Relationship between compressive strength and elastic modulus is shown in Fig. 4 with a regression curve. As exhibited in the difference in compressive strength of the specimens subjected to the standard curing, the difference in elastic modulus between specimens placed in summer and in winter was 3.5 MPa at a compressive strength of 180 MPa while no effects of temperature history were found in each batch.

Relationships between compressive strength and splitting tensile strength of sealed specimens of batches B2 and B4 are shown in Fig. 5. A general relationship common to specimens placed in summer and in winter is observed except for two points at a range from 100 to 140 MPa where compressive strengths of specimen placed in summer are smaller than that in winter.

2.4.2 *Autogenous shrinkage*

Autogenous shrinkage of specimens subjected to different temperature conditions is shown in Fig. 6. The temperatures after mixing of batches B1 and B3 specimens were 29.0 and 14.5 °C and the ambient temperatures were the same as those of the sealed specimens as shown in Fig. 3 while the temperatures after mixing of specimens subjected to the quasi adiabatic curing were 10, 20 and 30 °C. The difference in the thermal strain due to the difference in

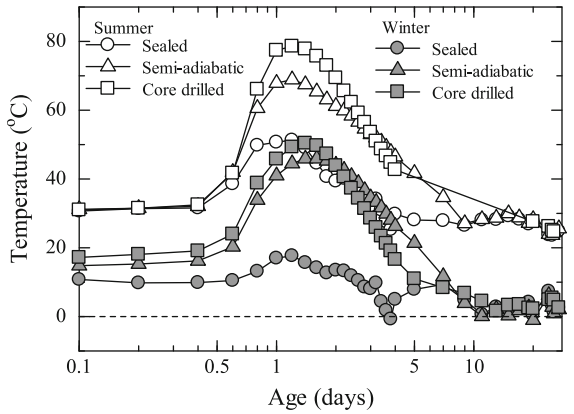

Fig. 3 Temperature histories of specimens for compressive strength

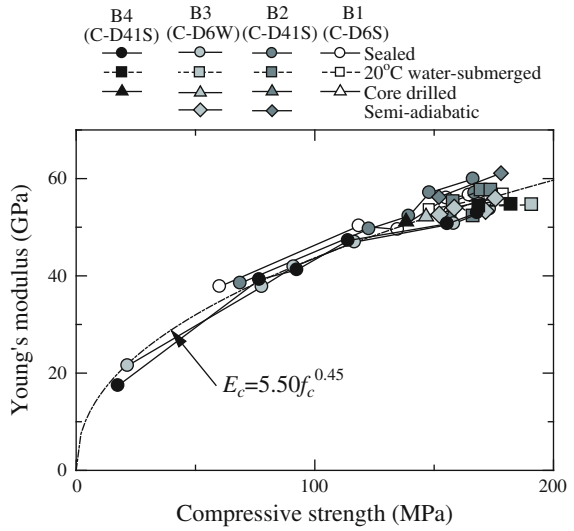

Fig. 4 Relationship between compressive strength and Young's modulus

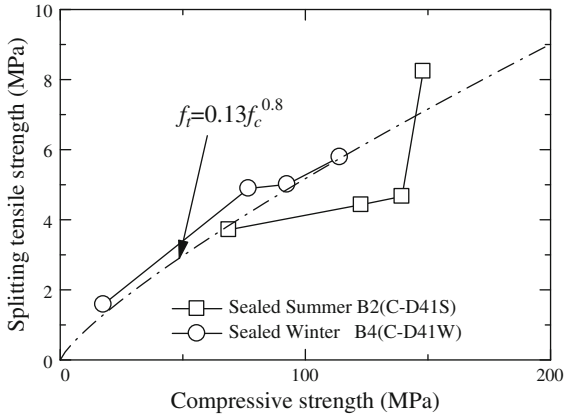

Fig. 5 Relationship between compressive strength and splitting tensile strength. Relative standard deviation of splitting tensile strength is 5.84 %

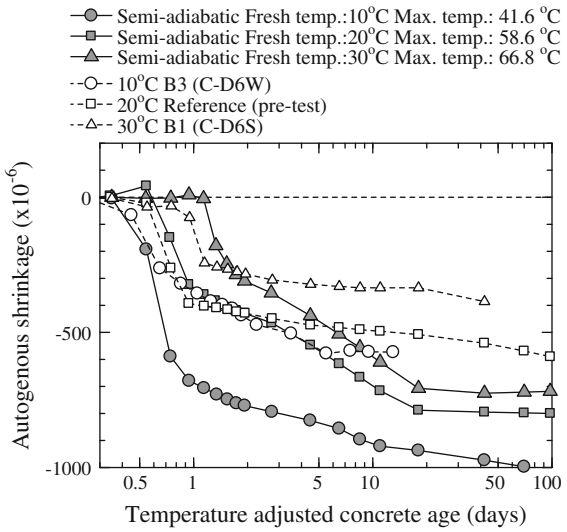

Fig. 6 Autogenous shrinkage of concrete under different temperature conditions. *Gray symbol* shows the autogenous shrinkage of concretes under different temperature at the fresh state (i.e., 10, 20, and 30 °C) and semi-adiabatic condition. *White square* showed autogenous shrinkage under 20 °C constant condition. *White triangle* and *circle* show the autogenous shrinkage of B1 and B3 respectively, whose room temperature is shown in Fig. 3

temperature after mixing and in the subsequent temperature history were converted to the strain at 20 °C assuming a constant thermal expansion coefficient of 10 × 10^{-6}/°C. The autogenous shrinkage was likely to increase as the temperature after mixing decreased for specimens with a constant (room temperature of 20 °C) temperature history and quasi adiabatic conditions, and those with a quasi adiabatic temperature history were larger than those with a constant temperature. This may be attributed to several conditions including a temperature dependency of hydration reactions and superplasticizing performance, and effects of mixing efficiency on the hydration reactions. These differences affect the cracking of members as described later.

2.4.3 *Strains in the column*

Changes in total strains and temperature histories inside of the C-D41S and C-D6S columns both placed in summer are shown in Figs. 7 and 8. The strains of the horizontal and vertical (axial) directions were measured with a mold type strain gauge and a foil type strain gauge and compared. The maximum temperatures were 75 °C at the center of the specimens and 50 °C at the mold surfaces in both specimens.

The vertical strain at the age of 1 day was expansive both at the reinforcing steel and at the neighboring concrete. Because this expansive strain was observed only in C-D41S and not in C-D6S, expansion of the reinforcement due to the cement hydration heat, whose effect was dependent on the reinforcement ratio of rebar, could pose expansion over the entire specimen.

Among specimens with different temperature after mixing, the specimen of 30 °C showed a delay in exhibiting autogenous shrinkage as shown in Fig. 6 though evaluated with the effective age. This may be attributed to a temperature dependency of superplasticizing performance, namely, the polycarboxylic acid type super plasticizer at higher temperatures increases the efficiency of dispersion of cement particles and prolongs the concrete setting. With this assumption, the volume change behavior of specimens can be interpreted as follows. At the age of 1 day when the autogenous shrinkage was observed, the modulus of elasticity of concrete around the steel reinforcement D41 was supposed to be small enough to undergo considerable restriction of the steel reinforcement resulting in an absence of large autogenous shrinkage strain at early ages, while subsequent increase in elastic modulus and concrete temperature led to a short term expansion and subsequent shrinkage. The vertical strain at the center of a specimen was a shrinkage strain probably because the restriction of steel

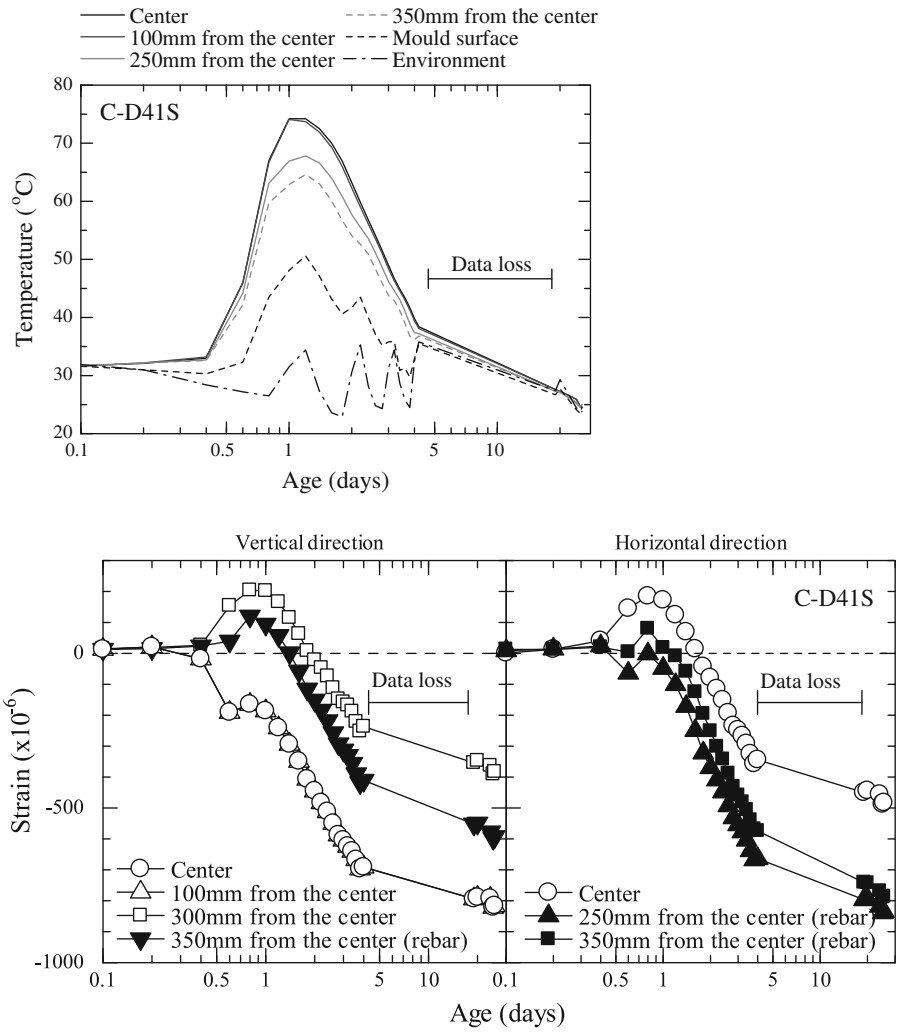

Fig. 7 Temperature and strain history in C-D41S

reinforcement could not extend over the central part due to undeveloped elastic modulus of the concrete.

Axial and horizontal shrinkage strains at the center of the specimens placed in summer were 816μ and 483μ for C-D41S and 715μ and 714μ for C-D6S. The axial shrinkage of C-D41S was remarkable at the center and became smaller at the perimeter parts while horizontal shrinkage strains showed larger shrinkage at the perimeter parts than that at the center. This tendency was confirmed both in C-D41S and C-D6S as shown in Fig. 6 and, if the autogenous shrinkage is isotropic, might be attributed to a tensile force acting horizontally at the center because autogenous shrinkage becomes larger as the temperature history higher. This assumption must be examined through the analytical study.

Changes in total strains and temperature histories inside of the C-D41W and C-D6W columns both placed in winter are shown in Figs. 9 and 10. The maximum temperature inside of the specimens was 50 °C. An abrupt change in strain at the age of 4 days was observed at the center of the C-D41W specimen due probably to cracking.

The effective age of a specimen with an age of 4-day and a temperature after mixing of 10 °C was estimated as 8.4 days at the center and 6.3 days at the perimeter region using the temperature history in Fig. 9. The splitting tensile strengths were 6.4 and

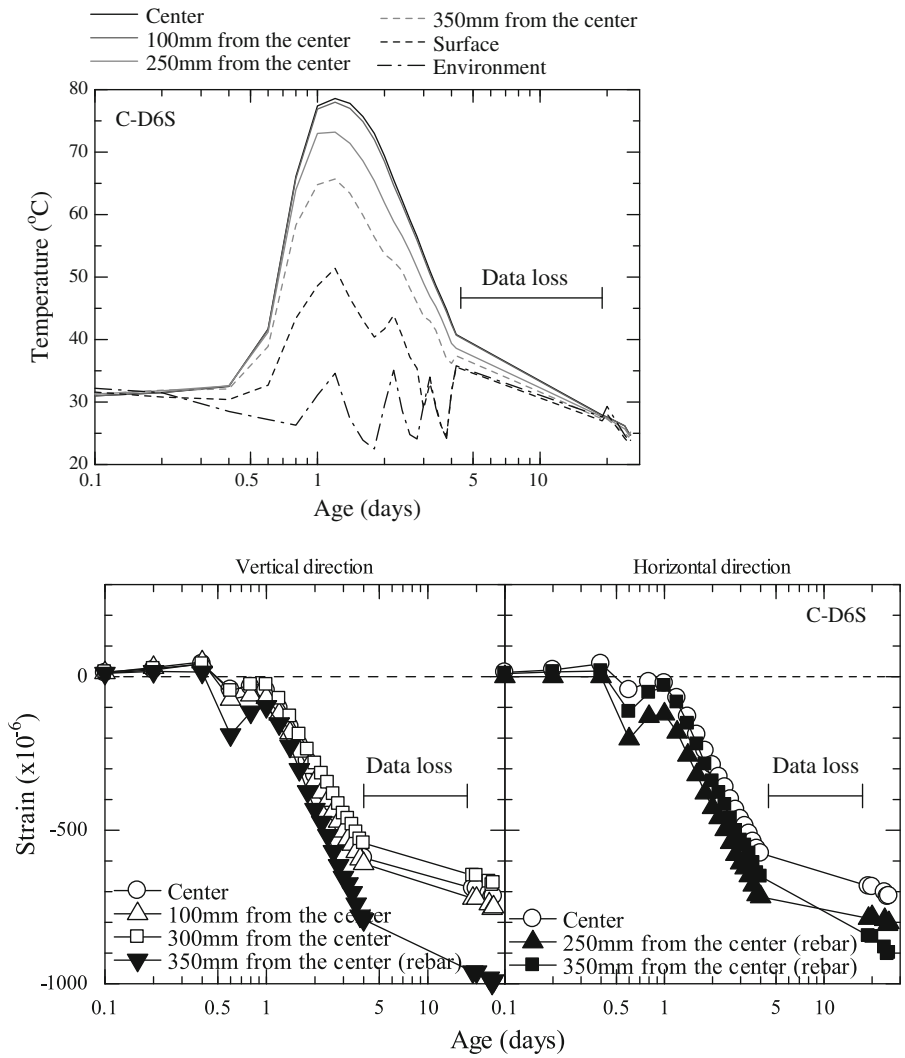

Fig. 8 Temperature and strain history in C-D6S

6.3 MPa respectively according to the regression equations in Fig. 5 and the autogenous strains were estimate to be 850μ and 600μ according to Fig. 6. This means that the major factor affecting cracking is a stress distribution due to autogenous shrinkage induced by hydration heat rather than the difference in the development of elastic modulus and tensile strength.

Unlike C-D41S, no indication of internal cracks were observed for C-D6W hence the major cause of the crack in C-D41S suppose to be the confinement of steel reinforcement superimposed on the force distribution in and outside of the specimen.

Temperature distributions inside of the specimens placed in summer and in winter are shown in Fig. 11 where no significant difference in temperature between the center and the near-surface part is confirmed while the positions showing the respective mean temperatures are significantly different: 200 and 360 mm from the center when placed in summer and in winter. This difference might have posed some changes in the confinement of steel reinforcement and could be a cause of the cracking.

2.4.4 Cracks in the column

Crack patterns around the main reinforcements at a cross-section (Section A in Fig. 1) of specimens C-D41S and C-D41W are shown in Fig. 12 and a photo of the cracks around a main reinforcement is shown in

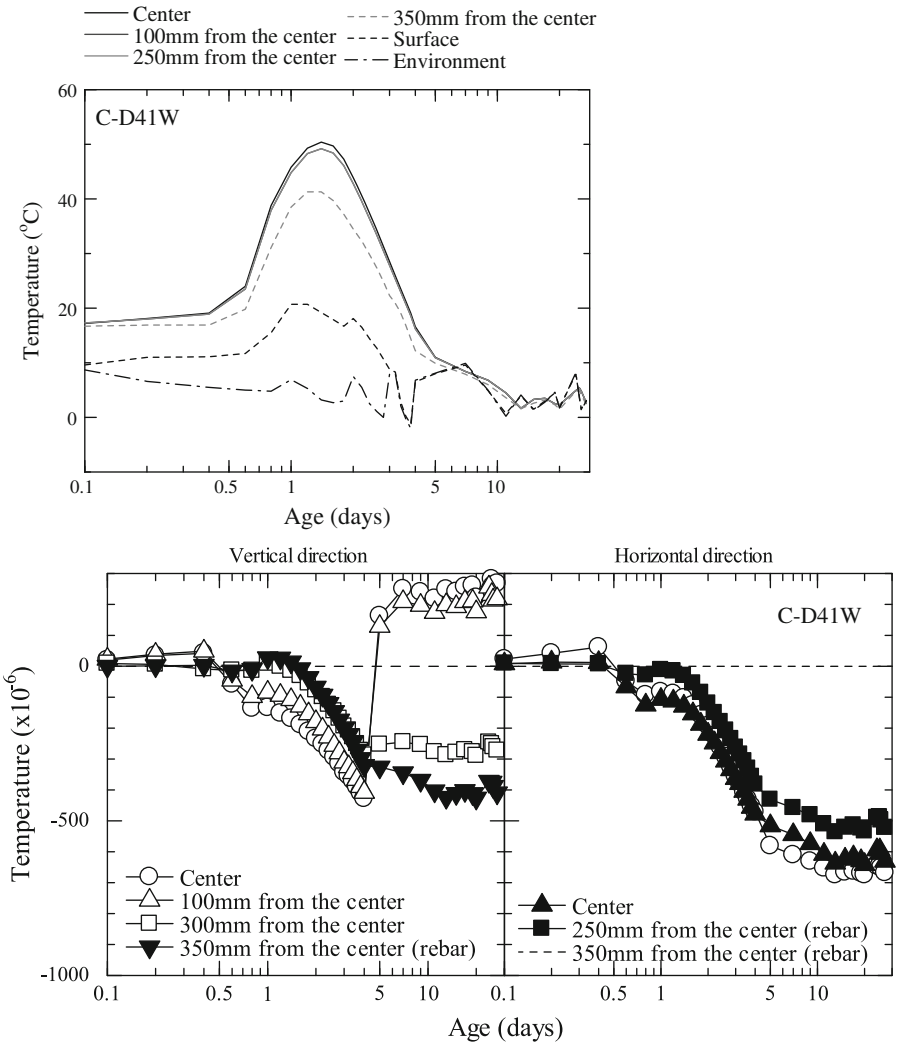

Fig. 9 Temperature and strain history in C-D41W

Fig. 13. The photo was taken during cutting with a diamond cutter when the cooling water was drying leaving the cracks still in wet and visible. The crack widths were all very small and less than 0.05 mm.

Crack patterns around the main reinforcements at the Section B of specimens C-D41S and C-D41W are shown in Fig. 14. A characteristic fine cracks were found not only around the main reinforcements but also around the shear reinforcements.

In the present study, it is difficult to ensure that the observed cracks were caused only by the volume change of concrete, because it is possible that high pressure is produced during sawing process. But it should be kept in mind that when the expansive additive and shrinkage reducing agent were added to the concrete, no crack around rebar was confirmed through the same experimental procedure [20]. This evidence means that the observed crack in this study was much affected by the volume change of concrete.

Surface cracks with a width ranging from 0.1 to 0.15 mm were observed for C-D41W, which developed 5 cm inward as shown in Fig. 15. Shallow honeycomb cracks formed on the surface of C-D6W while they became visible only during drying after applying a liquid such as water or acetone. Hence the cracks at the surface of C-D41W became actual when the autogenous shrinkage was restricted by the steel reinforcements.

Furthermore in C-D41W, large cracks formed inside perpendicular to the axial direction of the specimen,

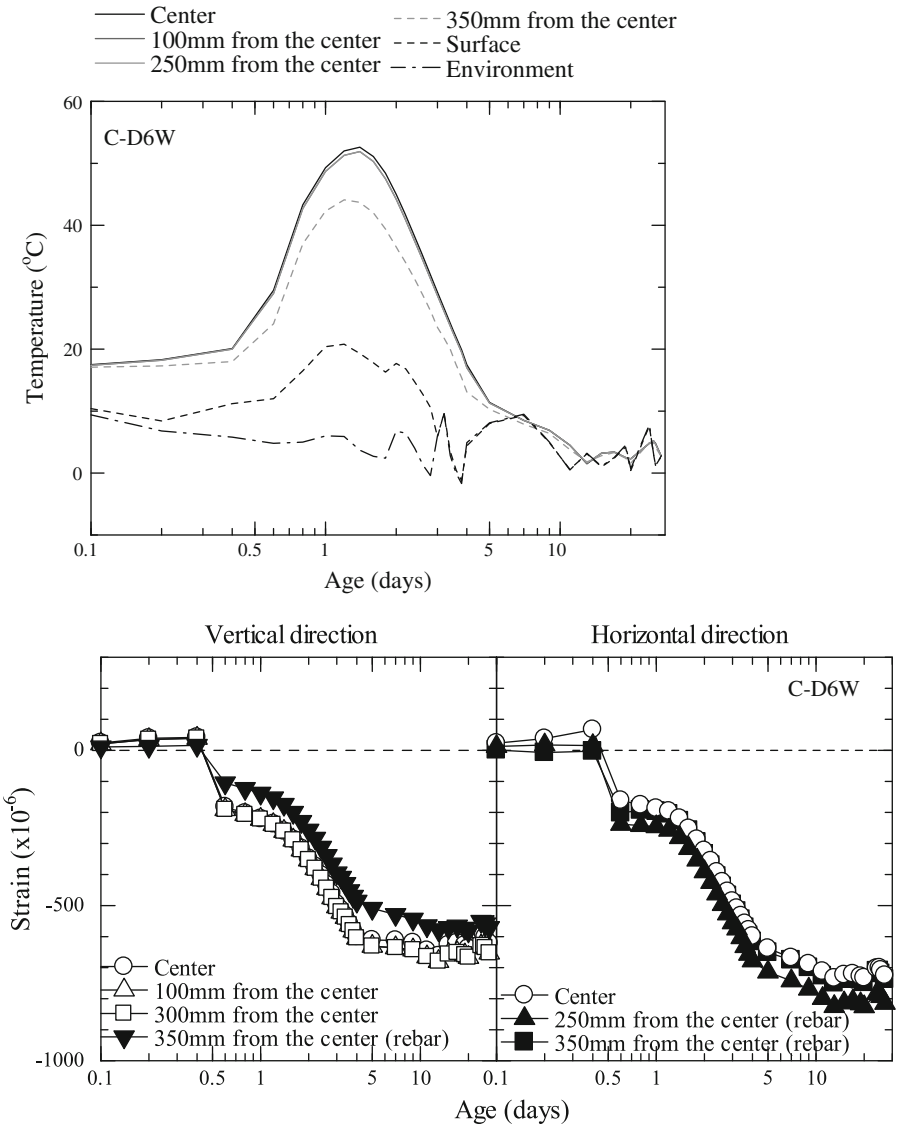

Fig. 10 Temperature and strain history in C-D6W

which may be what was measured with the mold type strain gauge as shown in Fig. 8. Because such cracks were not present in C-D6W, cause of the cracks may be attributed to a large autogenous shrinkage due to the high temperature history posed at the center and a restriction by the main reinforcement and the peripheral concrete where autogenous shrinkage was relatively small. The increase in autogenous shrinkage caused by the high temperature was limited to the central part of the specimen hence it is supposed that the cracks could not extend over the surface.

3 Analysis

Numerical analysis is attempted here to discuss the lateral stress of the column.

3.1 Material property model

As already mentioned, the relationship between effective age and strength can be given by the Eq. (1) and other properties are also presented.

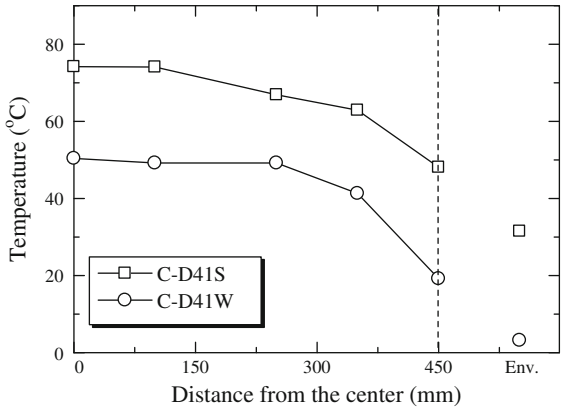

Fig. 11 Temperature distribution in the specimen at the temperature peak

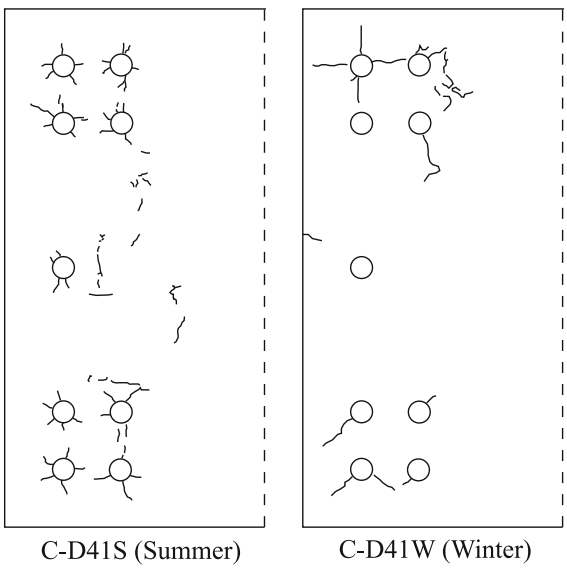

Fig. 12 Comparison of cracking pattern in the specimens on Section A

When the elastic modulus is evaluated as a function of age, the following equation of strength-elastic modulus relationship can be adopted,

$$E_c(t) = 5.5 \cdot f_c(t)^{0.45} \quad (2)$$

As mentioned in the previous section, autogenous shrinkage is affected by the temperature after mixing and the subsequent temperature history. However effects of the temperature history on the time-dependent behavior of the autogenous shrinkage cannot be estimated solely by the effective age. Thus the Eqs. (3) and (4) for the final value of autogenous shrinkage strain as a function of the maximum temperature during the temperature history were determined to fit the experimental values and used for the analysis.

Fig. 13 Cracking around deformed bar of C-D41S

$$\varepsilon_{sh}(t) = \varepsilon_{sh,max}\left\{1 - \exp\left(-(t-0.8)^{0.5}\right)\right\} \quad (3)$$

$$\varepsilon_{sh,max} = -\{320 + 8(T_{max} - 20)\} \quad (4)$$

where $\varepsilon_{sh}(t)$ is autogenous shrinkage strain (μ), T_{max} is the maximum temperature during the temperature history (°C), $\varepsilon_{sh,max}$ is the final value of autogenous shrinkage strain as a function of T_{max} (μ). Comparison of Eqs. (3) and (4) with the experimental values is shown in Fig. 16.

These equations are based on an assumption that the thermal expansion coefficient is constant and 10×10^{-6}/°C. When thermal analysis appropriately predicts temperature history, the total strain can be estimated by adding the autogenous shrinkage calculated with the Eqs. (3) and (4) and thermal strain calculated with the constant thermal expansion coefficient.

Creep equations used in this study are the reorganized version of the authors' existing study [19]. Among several engineering approaches to the creep strain taking account of the age at loading, a modified method of CEB-FIP Model Code 90 is simple but can show relatively precise prediction of stress for the high-strength concrete [4]. The method allows variable coefficient in the creep equation with age and introduces the ratio of the elastic strain with the 28-day elastic modulus to creep strain as the creep coefficient.

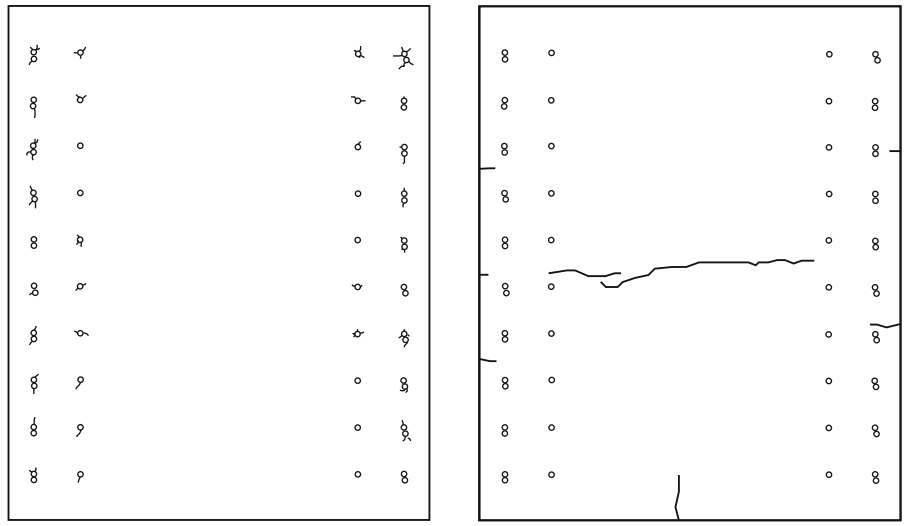

Fig. 14 Comparison of cracking pattern in the specimens on Section B

Fig. 15 Cracking on the surface of C-D41W

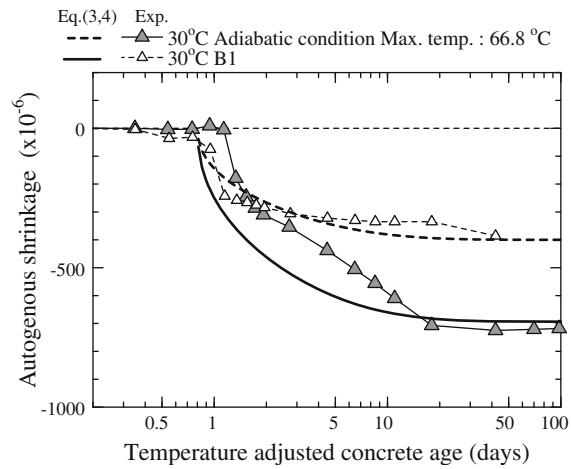

Fig. 16 Comparison of experimental data with predicted autogenous shrinkage by Eqs. (3) and (4)

The present study takes advantage of this approach and derives the following equations on the basis of experiments to evaluate the creep behavior of the ultra-high strength concrete.

$$\phi(t,t_0) = \phi_0\left(\frac{(t-t_0)/t_1}{\beta_h + (t-t_0)/t_1}\right)^{0.3} \tag{5}$$

$$\phi_0 = 0.15 + 5.2 \times \exp\left(-2.0 \times \left(E_c(t_0)/E_{c,28}\right)\right)$$

$$\beta_h \begin{cases} 49.4 \times (E_c(t_0)/E_{c,28}) - 13.2 & (E_c(t_0)/E_{c,28}) > 0.26 \\ 0.0 & (E_c(t_0)/E_{c,28}) \le 0.26 \end{cases}$$

where $\phi(t, t_o)$ is a ratio of elastic strain calculated with 28-day elastic modulus to creep strain (creep coefficient), ϕ_0 is the ultimate creep coefficient, β_h is a coefficient reflecting the effects of the age of loading, t is the effective age, t_1 is 1 day and $E_c(t_0)/E_{c,28}$ is a ratio of elastic modulus at the age of loading to that at 28 days. Numerical results are shown with solid lines in Fig. 17 in comparison with the experimental data

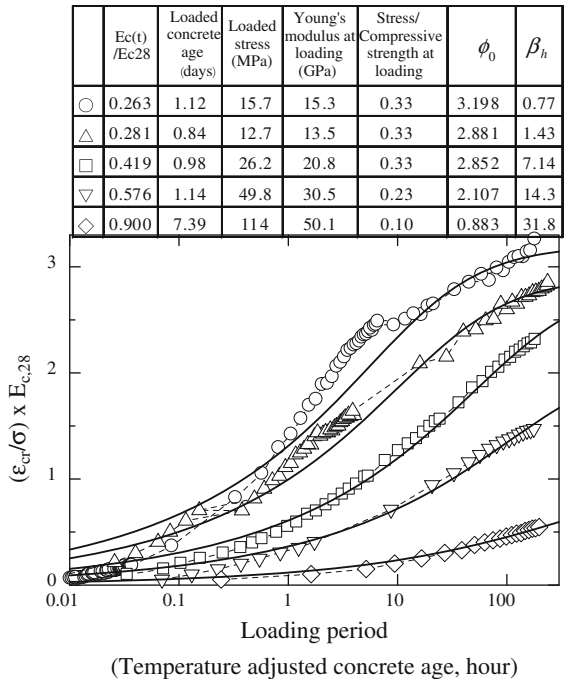

Fig. 17 Comparison of experimental creep coefficient data with predicted results by Eq. (5)

regarding concrete with the same mixture proportion as shown in Table 2. The experimental results of ϕ_0 and β_h [18] are shown with each regression curve in Fig. 18, where the past data at a water to binder ratio of 0.23 and 0.3 are cited [4] and good agreements are confirmed. Hence the proposed equations may be applicable as creep equations of high-strength concrete with a water to binder ratio ranging from 0.15 to 0.30.

The temperature increasing rate, as well as thermal conductivity and specific heat, used in the analysis

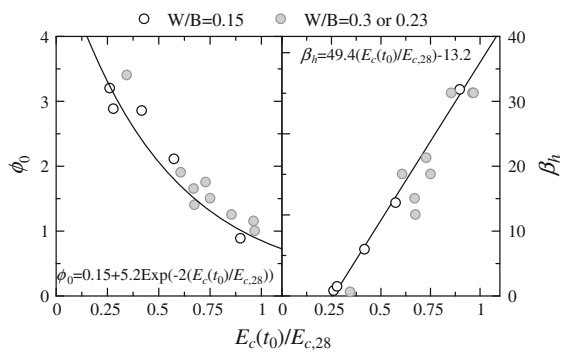

Fig. 18 ϕ_0 and β_h for creep coefficient curve of early age high-strength concrete

were determined to be most compatible with those obtained in experiments.

The thermal expansion coefficient of steel and elastic modulus were assumed to be 10×10^{-6}/°C and 200 GPa respectively while those used in the temperature analysis will be described later.

3.2 Numerical scheme

The heat conduction analysis was performed using 3D FEM based on Galerkin method. Meshing was made with an eight-point isoparametric element covering a 1/8 of the whole as shown in Fig. 19. The numbers of the contact points and elements are 1704 and 1331 and the main reinforcements were also regarded as a finite element while web reinforcements were not considered in the heat conduction analysis.

Adopted concrete and steel properties were thermal conductivity of 1.2 and 84 W/m K, specific heat of 1.1 and 0.453 J/g K, bulk density of 2.3 and 7.8 g/cm^3 respectively and the heat transfer coefficient over the mold surface was assumed to be 6.5 W/m^2 K. As a boundary condition, the measure outdoor temperatures were used for the analysis.

The stress analysis was performed using incremental 3D FEM developed by Sato and coworkers [4] capable of taking into account the effect of autogenous deformation and thermal strain by using the concept of equivalent nodal force. Using the result of the heat conduction analysis, mean temperatures of each element were calculated and the autogenous shrinkage histories were evaluated with Eq. (4) in each element.

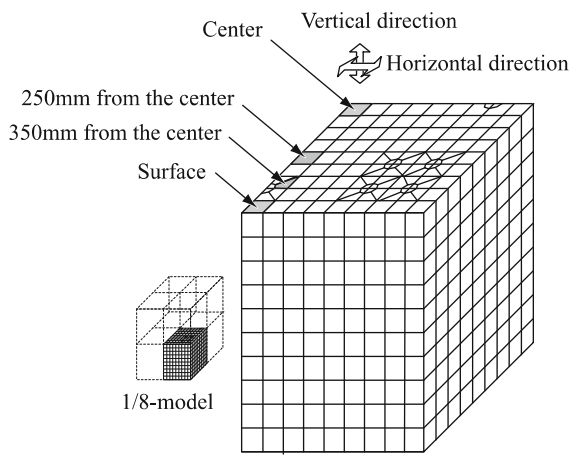

Fig. 19 Model for FE-analysis

Meshing was performed as shown in Fig. 19 and the hoop was modeled as a linear element responsible only for the axial force.

Because the fine cracks formed around the main reinforcements, bond degradation may be of concern, while a sufficient bond was assumed in this analysis.

The results of the present analysis will be discussed in terms of the mean value of three elements: the center, surface and the position 350 mm from the center as shown in Fig. 19. Hence the stress and strain are evaluated in terms of the mean value of eight nodes for the heat conduction analysis and that of eight integral points for the stress analysis.

3.3 Numerical results

3.3.1 Temperature history

As stated in the previous section, thermal properties of concrete and adiabatic temperature increasing rate were adjusted for the temperature history to be in compatible with the experimental results as shown in Fig. 20.

3.3.2 Strains and stresses

Strain distributions obtained with the analysis both for the vertical and horizontal direction of the column are shown in Figs. 21 and 22 respectively with reference to the strain at the placing. The strain at the position

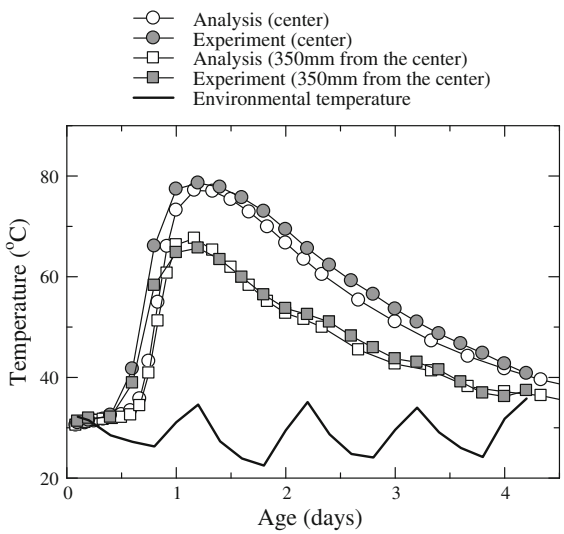

Fig. 20 Comparison of experimental temperature in the specimen with analytical results

350 mm from the center was an element belonging to steel but showed good agreement with that obtained with analysis. On the other hand, strains of concrete by analysis failed to reproduce the vertical settling and the horizontal dilatation observed by the age of 1 day and showed some difference in strain between those obtained by analysis and by experiment. The plastic behavior of concrete at very early stages, as discussed in Sect. 2.4.3, may be of some influence on the difference, and incorporation of the mechanism into analytical model is an issue in the future.

The present numerical analysis taking into account the temperature dependency of autogenous shrinkage was able to reproduce the following experimental results:

- The concrete strain at the center of the column was more expansive in the horizontal direction than that in the vertical direction.
- The vertical shrinkage strain was larger at the center than at the position 350 mm from the center.
- The horizontal shrinkage strain was larger at the center than at the position 350 mm from the center.

Because the above characteristic behavior of the specimens was compatible with the analytical results, discussion on the stress will be given on the basis of the analysis as follows.

The stress histories of concrete obtained with the analysis are shown in Fig. 23 where the entire cross-section is subjected to tensile stress in the vertical direction (left hand). The tensile stress is significant at the center of the column and very small at the surface. Two analytical studies were performed to discuss this behavior: the heat conduction analysis excluding autogenous shrinkage and the solo autogenous shrinkage stress analysis that assumed zero thermal expansion coefficient. Results are also shown in Fig. 23. The obtained thermal stress shows similar tendency with that of mass concrete: compressive stress at the central part and tensile stress at the surface with increase in temperature, and vice versa with decrease in temperature. The calculated autogenous shrinkage stress shows abrupt increase in tensile stress at the center of the column from early stages and gradual increase at the surface of the column, due to the restriction of the reinforcing steel. Because the autogenous shrinkage stress exceeds the compressive stress due to thermal expansion, tensile stress is dominant over the entire cross-section.

Stress history of the horizontal direction is shown in Fig. 23 (right hand). It was analytically shown that the

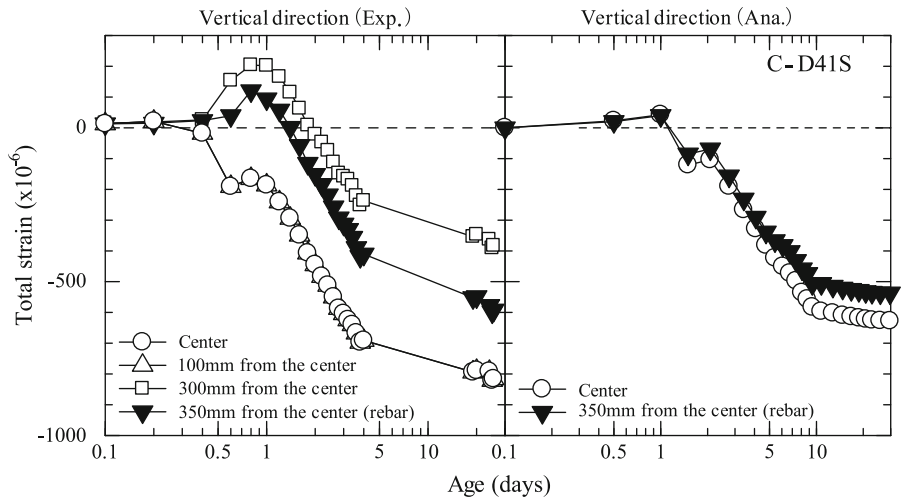

Fig. 21 Analytical results of total strain in vertical direction with experimental results

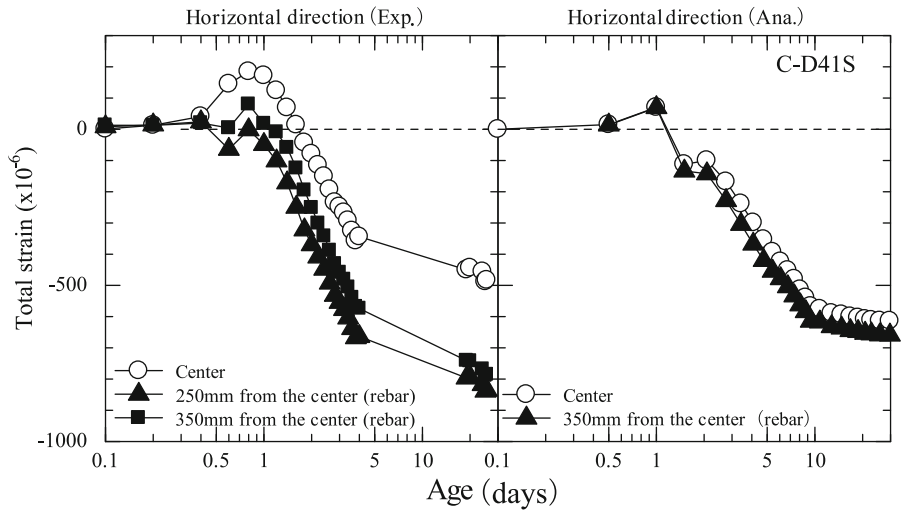

Fig. 22 Analytical results of total strain in horizontal direction with experimental results

concrete at the center of the column was subjected to tensile stress in the horizontal direction while that at the surface of the column was subjected to compressive stress. The separation of the thermal stress and the autogenous shrinkage stress was attempted to discuss the difference in the stress type. As shown in the mid and the bottom figures of Fig. 23 (right hand), thermal expansion is responsible for the compressive stress at the surface and the tensile stress at the center of the concrete while autogenous shrinkage stress at the surface was compressive at an early stage and subsequently approached to zero. This is a result of several interactions. First, the difference in autogenous shrinkage inside of the column induced stress because the higher temperature inside of the column accelerated the autogenous shrinkage. Next, the subsequent development of autogenous shrinkage at the surface part of the column mitigated the difference in the autogenous shrinkage strain resulting in the decrease in the stress. In these conditions, stress that had to be borne by concrete was tensile and in balance with the steel reinforcement.

As a result, it was confirmed that, among factors comprising the total stress, the autogenous shrinkage stress was dominant posing tensile stress at the center and compressive stress at the surface part of the concrete column.

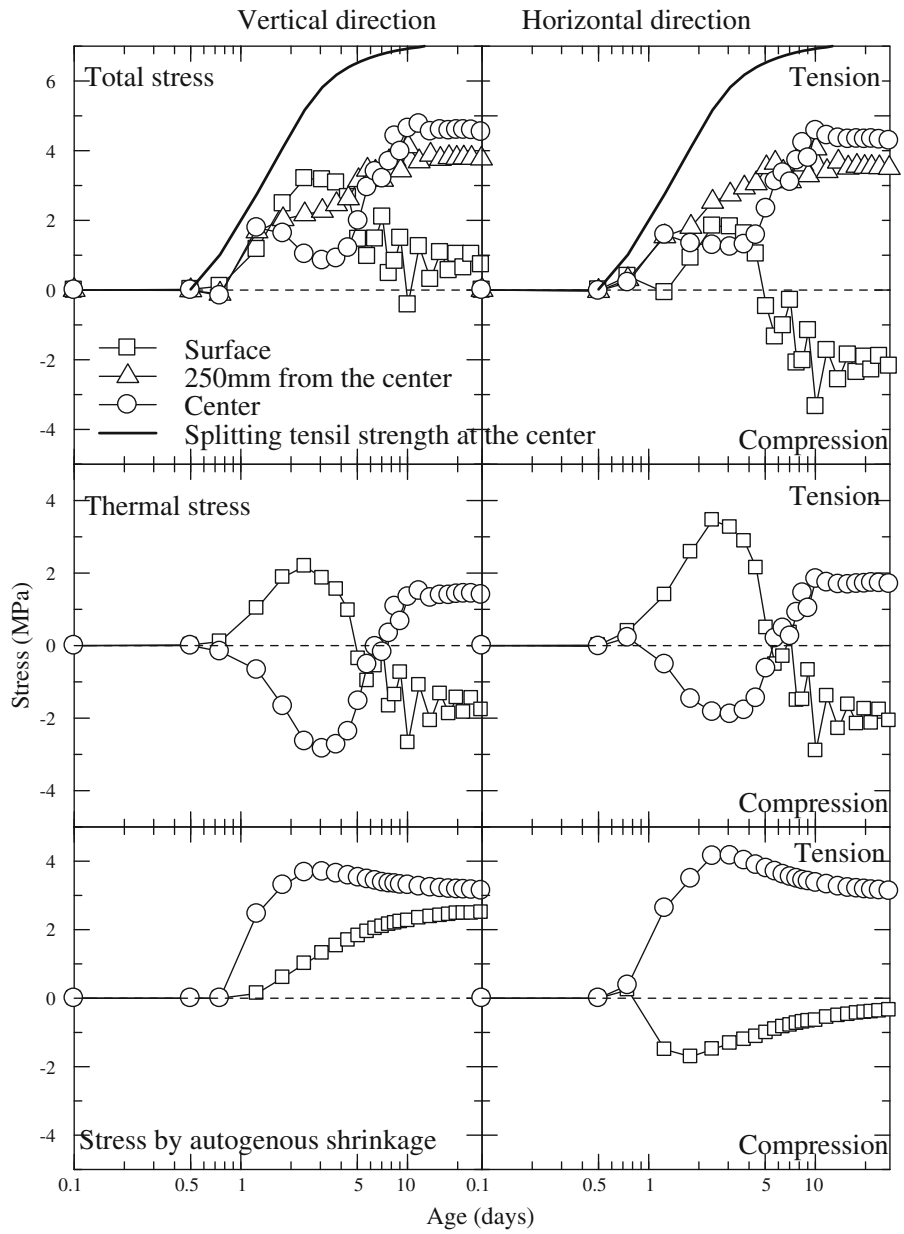

Fig. 23 Vertical and horizontal stress in the RC column

4 Discussion

4.1 Internal cracks

The internal cracks confirmed in C-D41W specimen were invisible on the surface. This is inconvenient when visual inspection is performed after the construction is completed. On the other hand, some positive effects such that crack propagation may be interrupted, when shear cracks intersects with the pre-existing crack, also be considered. Thus the evaluation of structural performance of the column, having preceding cracks due to autogenous shrinkage, is of significance.

Factors affecting such cracks are the temperature after mixing and internal temperature history and distribution that depend on the dimension of the member. A considerable autogenous shrinkage was

observed when the temperature after mixing was low and subjected to subsequent temperature history due to hydration heat liberation as shown in Fig. 6, which was supposed to be a cause of such cracks.

4.2 Silica fume addition

A fundamental study of the temperature sensitivity of silica fume and its effects on the autogenous shrinkage has been already performed [6], but studies concerning the reaction in high temperature and the resultant increase of autogenous shrinkage, especially in very low water to cement ratio, are still needed in depth as a coupled material–structure problem.

4.3 Cracks around the reinforcement

Cracks observed around the reinforcement as shown in Figs. 12 and 13 can be attributed to a tensile stress imposed at the peripheral direction of the steel reinforcement. A structural impact of the crack is an early spalling of the cover concrete [3] by which the strength degradation of members subjected to flexural loads, induction of buckling of the reinforcement and degradation of shear strength due to the bond failure are of concern. Possible countermeasures are short fiber reinforcement and a flexural strength design without cover concrete.

4.4 Experimental design

The conventional structural experiments with ultra-high strength concrete often used miniature models due the insufficient capacity of loading machines available. However, temperatures inside of the member were not realistic and the appropriate evaluation of structural performance might not be possible particularly for ultra-high strength full-scale members with considerable autogenous shrinkage. Experiments of the structural performance of concrete member with possible autogenous shrinkage need to be designed taking into account the amount of shrinkage and stress in the reinforcement before loading.

4.5 Lateral internal stress

As reported by Murata et al. [14], a vertical crack splitting of a high-strength concrete column into two blocks in the longitudinal direction was observed when subjected to a high axial force, and the degradation of the flexural strength was confirmed. Cracks in the column formed during loading after flexural yield are shown in Fig. 24 (left hand). Proposed mechanism of the cracking is shown in Fig. 24 (right hand) where lateral forces and axial loads after flexural yield are the influencing factors. According to Murata et al., shear force acting at the fracture plane was originated from the axial force and in proportional to the load, while tensile and shear strength of concrete were not in proportional to the axial force ratio determined in accordance with the compressive strength. Hence such a crack is specific to high-strength concrete and rare in the normal concrete.

Internal stress originated from the early-age autogenous shrinkage and temperature history can produce such a vertical crack even before flexural shear forces are applied. Also as shown in Sect. 3.3, the internal vertical crack may be still invisible on the surface because the surface part is subjected to enough compressive stress.

Even though the vertical crack, originated from autogenous shrinkage and temperature history, is absent, the vertical splitting after flexural yield may still occur due to the lateral stress under a low axial load.

After vertical cracking, the stress distribution in a cross-section will be dissolved leaving a partial loss of the area.

Because the ultra-high strength concrete columns are preferably used for the lower stories of high-rise buildings and subjected to variable axial loads, the internal lateral stresses discussed above may not be negligible in the structural design. Future tasks are the exploration of a shear reinforcement design principle capable of assuring the unity of structural elements subjected to considerable autogenous shrinkage stresses, and to give concrete additional toughness using short fibers.

5 Concluding remarks

Early-stage stresses and cracking of full-scaled ultra-high strength concrete columns, placed in summer and in winter, were experimentally studied. Major findings are as follows.

(1) Autogenous shrinkage of ultra-high strength concrete changed according to the temperature

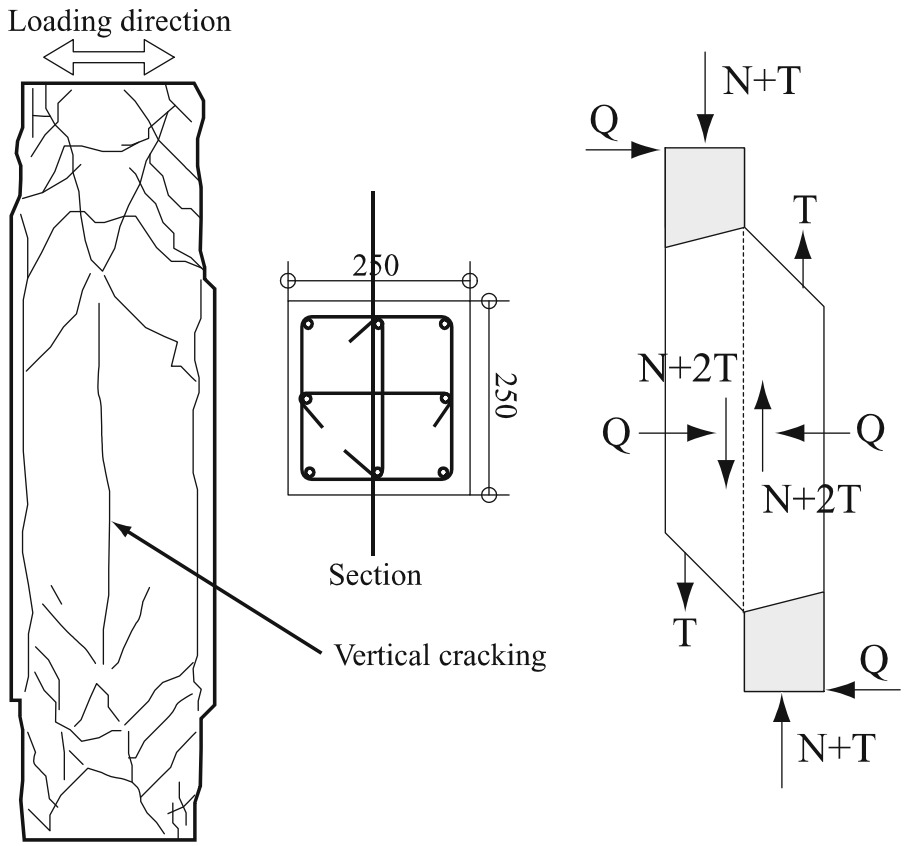

Fig. 24 Vertical splitting of RC column reported by Hiraishi et al. and their proposed mechanism of it

after mixing and subsequent temperature history. Autogenous shrinkage showed significant increase when subjected to high temperature history due to hydration heat liberation and also increased when the temperature after mixing was low. Unlike the belief that autogenous shrinkage increases with an increase in the maximum temperature during early-stage temperature history, it depended upon both the maximum temperature and the temperature after mixing, leading to a higher cracking risk for concretes placed in winter.

(2) The full-scaled model column placed in winter showed large autogenous shrinkage. Because the autogenous shrinkage was restricted by the reinforcement, cracks were observed on the surface and inside of the column, and around the reinforcement. The internal cracks were originated from the large autogenous shrinkage of the central part of the concrete column when underwent the high temperature history and the restriction both by the reinforcement and the other parts of concrete with smaller autogenous shrinkage. The internal cracks remained inside of the concrete column and were thus not accessible by visual inspections after the completion, posing a problem with quality control. Influences of the internal cracks on the structural performance and control of the internal cracking need to be studied.

(3) Cracks around the main reinforcement were observed. This may imply possible structural failures such as early spalling of cover concrete, degradation of flexural strength associated with reinforcement bucking and decrease in shear strength due to bond degradation. Because the cracks are supposed to become significant with an increase in autogenous shrinkage under high temperature histories due to hydration heat liberation, it is very likely that miniature model column, often used in flexural–shear experiments, does not reproduce the high-risk

situations. Material properties taking into account temperature history and experiments with miniature column specimen paying attentions to the similarity of bar arrangement need to be investigated.

(4) When using an ultra-high strength concrete column with a large cross section, lateral tensile stress was found to be present at the central part due to a large autogenous shrinkage associated with high temperature history. This may lead to the bi-block splitting of the column at a high axial load. An appropriate shear reinforcement design to ensure the unity of a structural element needs to be researched.

References

1. Bentur A, Igarashi S, Kovler K (2001) Prevention of autogenous shrinkage in high-strength concrete by internal curing using wet lightweight aggregates. Cem Concr Res 31:1587–1591
2. CEB-FIP (1991) Model code 1990, Thomas Telford
3. Collins MP, Mitchell D, MacGregor JG (1993) Structural design considerations for high-strength concrete. Concr Int 15:27–34
4. Ito H, Maruyama I, Tanimura M, Sato R (2004) Early age deformation and resultant induced stress in expansive high strength concrete. J Adv Concr Technol 2:155–174
5. Japan Concrete Institute (2008) Guidelines for control of cracking of mass concrete. JCI, Tokyo
6. Jensen OM, Hansen PF (1999) Influence of temperature on autogenous deformation and relative humidity change in hardening cement paste. Cem Concr Res 29:567–575
7. Jensen OM, Hansen PF (2001) Water-entrained cement-based materials: I. Principle and theoretical background. Cem Concr Res 31:647–654
8. Katayose N, Takamori N, Nishida H, Teraoka M (2006) Mechanical properties and autogenous shrinkage behavior of high strength concrete at early age. Proc Jpn Concr Inst 28:497–502 (in Japanese)
9. Kovler K, Jensen OM (2007) Internal curing of concrete, State-of-the-art report of RILEM technical committee 196-ICC, Report 41
10. Lura P, van Breugel K, Maruyama I (2001) Effect of curing temperature and type of cement on early-age shrinkage of high performance concrete. Cem Concr Res 31:1867–1872
11. Lura P, Jensen OM, Weiss J (2009) Cracking in cement paste induced by autogenous shrinkage. Mater Struct 42: 1089–1099
12. Maruyama I, Sato R, Suzuki M (2005) Verification of soundness of HPC in RC members. Summaries of technical papers of annual meeting, Architectural Institute of Japan, 2005.9, Osaka, PP 625–626 (in Japanese)
13. Maruyama I, Kameta S, Suzuki M, Sato R (2006) Cracking of high strength concrete around deformed reinforcing bar due to shrinkage. In: Kovler K (ed) International RILEM-JCI seminar on concrete durability and service life planning, RILEM Publications S. A. R. L., Ein-Bokek, pp 104–111
14. Murata Y, Kurihara M, Yagenji A, Kaminosono T, Hiraishi H (1991) Vertical split of high-strength RC columns. Summaries of technical papers of annual meeting, Architectural Institute of Japan, Osaka, Structures II, pp 155–156 (in Japanese)
15. Paillere AM, Buil M, Serrano JJ (1989) Effect of fiber addition on the autogenous shrinkage of silica fume concrete. ACI Mate J 86:139–144
16. Sato R, Tanaka S, Hayakawa T, Tanimura M (1999) Experimental studies on reduction of autogenous shrinkage and its induced stress in high strength concrete. In: Proceedings of the 2nd international research seminar on self-desiccation and its importance in concrete technology, Lund, pp 163–171
17. Schrage I, Mangold M, Sticha J (1992) An approach to high-performance concrete in Germany. In: Fourth CANMET/ACI international conference on fly ash, silica fume, slag, and natural pozzolans in concrete, Istanbul, Supplementary Papers, pp 493–511
18. Suzuki M, Nakase H, Maruyama I, Sato R (2005) Effect of temperature on self-stress of expansive ultra high strength concrete. Cem Sci Concr Technol 59:375–382 (in Japanese)
19. Suzuki M, Maruyama I, Amacho S, Sato R (2006) A Study on deformation and resultant induced stress in expansive-ultra high strength concrete. Proc Jpn Concr Inst 28: 563–568 (in Japanese)
20. Suzuki M, Maruyama I, Nakase H, Sato R (2009) Reduction of self-induced stress and resultant cracks in reinforced ultra high-strength concrete column by dosage of expansive additive and shrinkage reducing agent. J Struct Constr Eng Trans AIJ 635:1–10 (in Japanese)
21. Tazawa E, Miyazawa S (1992) Autogenous shrinkage caused by self-desiccation in cementitious material. In: 9th international congress on the chemistry of cement, New Delhi vol 4, pp 712–718
22. Tazawa E, Miyazawa S (1995) Experimental study on mechanism of autogenous shrinkage of concrete. Cem Concr Res 25:1633–1638
23. Tazawa E, Matsuoka S, Miyazawa S, Okamoto S (1994) Effect of autogenous shrinkage on self stress in hardening concrete. In: International RILEM symposium on thermal cracking in concrete at early ages, Munich, pp 221–228
24. Tsutsui H, Sato R, Xu M (1996) A study on stress due to autogenous shrinkage in high-strength concrete. JCA Proc Cem Concr 50:478–483 (in Japanese)